Measurements of Rayleigh-Taylor Growth Rate of Planar Targets Irradiated Directly by Partially Coherent Light

K. Shigemori, H. Azechi, M. Nakai, M. Honda, K. Meguro, N. Miyanaga, H. Takabe, and K. Mima
Institute of Laser Engineering, Osaka University, 2-6 Yamada-Oka, Suita, Osaka, 565 Japan
(Received 3 July 1996)

We report the first measurements of laser-driven Rayleigh-Taylor instability at the linear growth regime in an imprint-free condition. Initially rippled polystyrene foils were irradiated by the partially coherent light. We measured temporal evolution of areal-density perturbation by the face-on x-ray backlighting technique. The observed maximum growth factor was nearly 50. We also measured the acceleration of the irradiated foil. The growth rate was approximately 50% of the classical growth rate. These experimental results were well reproduced by a two-dimensional simulation coupled with the Fokker-Planck treatment of electron heat transport. [S0031-9007(96)02068-6]

PACS numbers: 52.35.Py, 52.50.Jm, 52.70.La

As is well known, hydrodynamic instabilities, such as the Rayleigh-Taylor (RT) instability [1], play an important role in inertial confinement fusion (ICF) implosions [2] and supernova explosions [3]. In ICF implosions, initial perturbations on the target surface will grow due primarily to the RT instability, resulting finally in fuel-pusher mixing that degrades the implosion performance. To limit the mixing within an acceptable level, good understandings of the RT instability are necessary. Since the initial perturbation amplitude in most ICF targets and supernovae are much less than the wavelength, the perturbation first grows exponentially with time up to a time when the amplitude becomes about 10% of the perturbation wavelength, and after that the growth tends to saturate [4]. Thus the RT instability in the linear regime gives the largest growth of the perturbation. The growth rate of the RT instability is expected to be suppressed as the perturbation is removed away from the unstable region by material ablation [5]. The theoretical RT growth rate γ that includes the ablation effect is given by the Takabe formula [6]: $\gamma = 0.9\sqrt{kg} - \beta k\dot{m}/\rho$, where k is the wave number of the perturbation, g is the acceleration, $\dot{m}$ is the mass ablation rate per unit surface, ρ is the density at the ablation front, and β is the constant depending on the structure of the ablation surface. This structure may be different for two major schemes of ICF: direct-drive and indirect-drive schemes. For indirect-drive (x-ray-drive) ablation, the measurements of the linear RT growth are consistent with β value of 1–2 [7]. Several experimental investigations [8] were also carried out about RT instability in directly driven targets. However, to date, there are few works [9] on the RT growth in the linear growth regime, because the initially imposed perturbation is easily influenced by imprinting of nonuniformity in laser irradiation.

In this Letter, we describe the first measurements of the growth rate of the RT instability at the linear regime in an imprint-free condition. Initially corrugated plastic foils were irradiated uniformly by the partially coherent light (PCL) [10] with time averaged nonuniformity of about 2%. The perturbation wavelength was fixed to be 60 μm, whereas only the amplitude was varied from 0.1 to 1.0 μm. We observed areal-density perturbation with the face-on x-ray backlighting technique. The maximum growth factor was 50. We also measured the trajectory of the target, and thus the target acceleration, in order to evaluate the classical growth rate. Observed growth rate was 50% of the classical value, $\sqrt{kg}$. The interpretation of the growth rate reduction is that high energy electrons preheat the target via nonlocal heat transport, thereby reduce the target density, and thus increase the ablation velocity. The experimental growth rate is in better agreement with the simulation results with the nonlocal heat transport described by the Fokker-Planck (FP) equation [11] than those with the classical heat transport by the Spitzer-Härm (SH) model [12].

A schematic view of the experimental setup is shown in Fig. 1. The targets were made of polystyrene (PS) with a density of 1.06 g/cm^3 and a thickness of 16 μm. The perturbation wavelength was 60 μm and amplitudes were 0.1 ± 0.02, 0.3 ± 0.05, and 1.0 ± 0.1 μm. Sinusoidal perturbations were imposed on the laser irradiation side by the thermal-press method [13]. As for the drive beam, we used frequency-doubled ($\lambda = 0.53$ μm) PCL for uniform irradiation. The PCL was generated from optical fibers [14], amplified by the GEKKO XII glass laser system [15]. The characteristics of the PCL at 0.53 μm wavelength were a bandwidth of 0.2 nm, a beam divergence of 64 times diffraction limit, and a one-dimensional

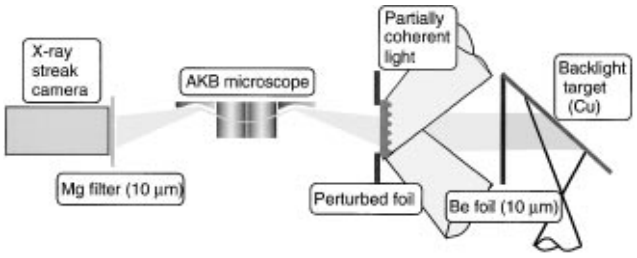

FIG. 1. Schematic view of the experimental setup for the measurement of areal-density perturbation.

 0031-9007/97/78(2)/250(4)$10.00

angular spectral dispersion of 478 μrad/nm. The irradiated laser beam was further smoothed by the random phase plate [16]. The time-integrated focal pattern had a nearly flat shape with a 600 μm diameter (FWHM) and a 2% (rms) intensity fluctuation from the smooth envelope. The PCL has two-step wise shape with a 1.8 ns foot pulse of 0.7×10^{13} W/cm^2 intensity followed by a 1.8 or 2.2 ns main pulse of 0.7×10^{14} W/cm^2 intensity. This pulse shape was obtained by three beams with one beam proceeded by 1.8 ns. Both foot and main pulses had a 0.05 ns rise time and a 0.15 ns fall time. We defined the time zero ($t = 0$) as the time of the first half maximum of the main pulse.

Areal-density perturbations were measured by face-on x-ray backlighting. A Cu target was irradiated by two beams to generate backlighting x rays. The Cu backlighter was located at 3 mm from the PS target. To cover a long time evolution, one of the two beams preceded the main drive pulse by 0.4 ns. The backlighter lasers were focused on the target with a 500 μm spot size at an intensity of $\approx 1 \times 10^{14}$ W/cm^2. X-ray spectra from the backlighter target, measured with a TlAP spectrometer, consist of dominant lines at 1.1–1.3 keV and weak lines above 1.3 keV. To eliminate a preheating of the foil by soft x rays emitted from the backlighter, a 10 μm thickness Be shield was placed between the backlighter and the perturbed foil target. The measured x-ray spectra (1–1.8 keV) indicates that the preheating by the backlighter x ray is expected to be negligible. The transmitted x rays were imaged by an advanced Kirkpatrick-Baez microscope [17] with a 24.6 magnification onto a CuI photocathode of an x-ray streak camera. A Mg filter of 10 μm thickness was used in front of the streak camera to block a high energy x-ray band with its K-shell absorption ($\geq$1.3 keV). The temporal resolution was nearly 90 ps. The spatial resolution function (line-spread function) $R(u)$ of the whole diagnostic system was obtained from backlit gold-grid images. Assuming that the resolution function is given by the sum of two Gaussian functions, $R(u) = [1/(1 + \alpha)]\{\exp[-u^2/(2\sigma_1^2)] + \alpha \exp[-u^2/(2\sigma_2^2)]\}$, we got $\alpha = 0.009$, $\sigma_1 = 12.8$ μm, $\sigma_2 = 62.8$ μm at the target plane. Using a two-step PS target with a thickness difference of 7–20 μm, the effective mass absorption coefficient was measured to be $\mu_{\mathrm{CH}} = (1.03 \pm 0.05) \times 10^3$ cm^2/g, being in good agreement with the tabulated coefficient at 1.2 keV for neutral PS [18].

First, we observed no perturbation even at the end of the drive ($t \approx 2$ ns) for a blank PS foil with the same thickness irradiated with the same PCL pulse as those for the perturbed PS foil. This implies that the initial imprinting at wavelength similar to the preimposed wavelength is at most 0.5 μm/50 = 0.01 μm, since the detection threshold of the present backlight system is about 0.5 μm for the 60 μm perturbation wavelength, and measured growth factor is about 50 at $t = 2.0$ ns.

Second, we measured the trajectory of the irradiated foil using the side-on x-ray backlighting to determine the acceleration g. We used Al targets to generate 1.5–1.7 keV x rays. The backlit foil was imaged by a slit (10×50 μm^2) onto an Au photocathode of an x-ray streak camera. The target was a flat PS foil of 16 μm thickness with no perturbation. In the side-on geometry, the laser-irradiated surface may be hidden by the surrounding weakly irradiated surface. To avoid this, the target width was restricted to be 300 μm over which the laser intensity changed by only 15%. We determined the target position from the point of the maximum x-ray attenuation. Figure 2 shows the target trajectories from the experiment and from the 1D simulation "ILESTA" [19]. The experimental trajectory was fitted with a second-order polynomial, giving the acceleration of $g = (5.0 \pm 0.5) \times 10^{15}$ cm/s^2.

Raw streaked images by the face-on experiment are shown in Figs. 3(a)–3(c). The areal-mass-density perturbation is recorded as a contrast of the transmitted x-ray image. The line scans for different observation times are shown in Fig. 3(d). The data were time integrated for 100 ps, approximately equal to the temporal resolution. The areal-density perturbation amplitudes were iteratively obtained by fitting a calculated distribution of the transmitted x-ray with the experimental results. The fitting function is a convolution of the transmitted x-ray distribution with the resolution function, as is given by $I(x) = \int R(x - u) I_0(u) \exp[-\mu_{\mathrm{CH}} \sum_n (\rho l)_n \cos(nku)]\, du$, where $I_0(u)$ is a spatial distribution of the backlighter emission after passing the mean target thickness, μ_{CH} is the effective mass absorption coefficient, ρl is the foil areal density, and n means the nth order harmonic component. The intensity distribution of the backlighter $I_0(x)$ was well fitted by a superposition of two Gaussian functions.

Figure 4 shows the growth factors, defined as the measured areal-density perturbation divided by the initial value, from three target shots with varying initial amplitude of $a_0 = 0.1$, 0.3, and 1 μm. Perturbation amplitudes are analyzed with only the fundamental mode. The maximum growth factors were 50 ± 5, 15 ± 2, and 7 ± 1.5 for $a_0 = 0.1$, 0.3, and 1 μm, respectively. The areal density perturbation already grows by a factor of 3–4 of the initial perturbation before the time zero because of the rippled-shock propagation in the target

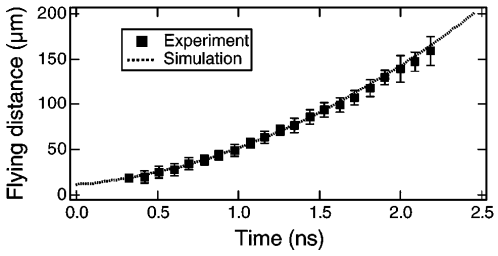

FIG. 2. The trajectories of the foil from the experiment and the simulation.

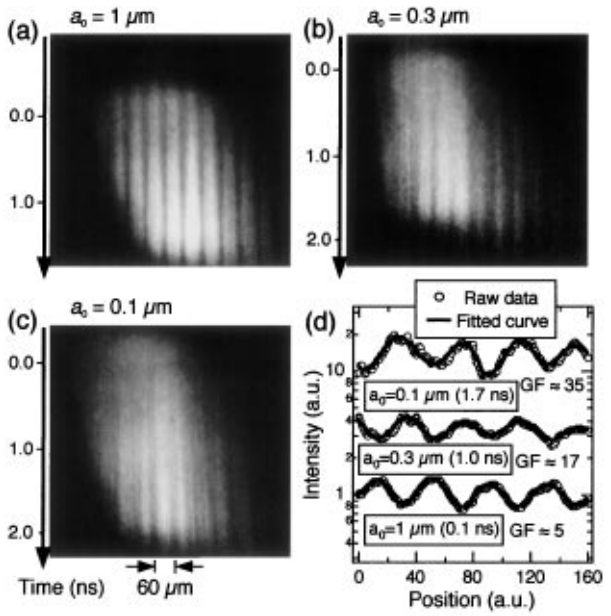

FIG. 3. The streaked backlighting images for (a) $a_0 = 1$ μm, (b) $a_0 = 0.3$ μm, and (c) $a_0 = 0.1$ μm. (d) The line scans for different initial amplitudes at times when the amplitudes are comparable each other. Data are well fitted by a single-mode sinusoidal curve.

[20] and of the weak RT instability at the foot-pulse region. For the small and medium initial amplitude cases ($a_0 = 0.1$ and 0.3 μm), the raw data are well fitted by a single-mode sinusoidal perturbation. In the case of large initial amplitude ($a_0 = 1.0$ μm), the higher harmonics become important. We also obtained the fundamental and the higher harmonics for each case. The second harmonics arises at 0.5 ns for the $a_0 = 1.0$ μm case, at 1.5 ns for the $a_0 = 0.3$ μm case, respectively. For the smallest amplitude case ($a_0 = 0.1$ μm), no second harmonics appear by the very end of time. The growth factors for the small initial amplitude case, 0.1 and 0.3 μm, are well fitted by an exponential curve (the dashed line) with the growth rate of $\gamma_{\text{exp}} = 1.2 \pm 0.1\ \text{ns}^{-1}$. On the other hand, the classical growth rate of the RT instability is calculated to

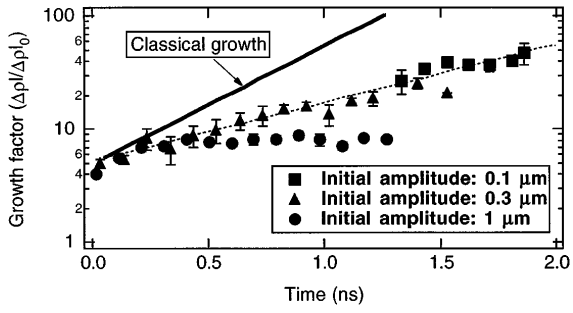

FIG. 4. The growth factor as a function of time for three different amplitudes. A solid line, which is offset arbitrarily, shows the classical growth. The ratio of the measured to the classical growth is $\gamma_{\text{exp}}/\gamma_{\text{classical}} \approx 0.5$.

be $\gamma_{\text{classical}} = \sqrt{kg} = 2.4 \pm 0.1\ \text{ns}^{-1}$, where the acceleration is corrected to be $g = (5.4 \pm 0.5) \times 10^{15}\ \text{cm/s}^2$ to take into account the small difference of the laser intensity from that in the side-on backlighting experiment, described previously. The solid line in Fig. 4 shows the classical growth. The measured growth rate is approximately 50% of $\gamma_{\text{classical}}$.

To compare the measured growth rate with the theoretical growth rate given by the Takabe formula, mass ablation rate $\dot{m}$ was also evaluated. Our mass ablation measurement is based on the fact that when mass ablation occurs x-ray transmittance increases as the residual areal mass density is decreased, whereas the ablated corona plasma does not absorb keV x rays due to the absence of bound electrons. This measurement was made from the time varying x-ray intensity transmitted through a flat PS foil, irradiated at the identical experimental configuration as that of the face-on experiment. The time variation of the incident x-ray intensity was separately measured using an unirradiated PS foil and was found to be nearly constant with $\pm 10\%$ variation. The measured mass ablation rate was $((3.5 \pm 0.3) \times 10^5\ \text{g/cm}^2\,\text{s}$. The ILESTA-1D shows less mass ablation rate but not much.

Among various mechanisms to reduce the growth rate, the effect of density gradient is first ruled out because the simulated density scale length of <1 μm is much smaller than the perturbation wavelength. The finite thickness effect [7,21] may contribute only a few percent reduction of the growth rate. The ablation effect is commonly considered to be the dominant stabilization mechanism. For quantitative comparison, we substitute experimentally measured values of γ, $\dot{m}$, g, and k into the Takabe formula, giving $\beta/\rho = 2.6 \pm 0.8$. Further substitution of the simulated ablation density of 3.5(at $t = 0.5$ ns)–2.5(at $t = 1.8$ ns) g/cm^3 would give an anomalously large value of $\beta = 9.1 \pm 2.8$–6.5 ± 2.0 compared to the prediction of $\beta = 3$–4 [6]. Complementary, numerical analysis of the RT growth using simulated values of $\dot{m}(t)$, $\rho(t)$, $g(t)$, and $\beta = 3$–4 gives growth curves similar to the classical growth (solid line in Fig. 4), being in disagreement with the experiments. Therefore, the experiment indicates that the β value is much larger than expected or the ablation density is lower than the simulated value.

One probable mechanism to reduce the ablation density is preheating due to nonlocal heat transport. The electron-electron mean-free path is calculated to be 10 μm at the critical density for the electron temperature $T_e \approx 1.8$ keV calculated from the ILESTA-1D, and is comparable to the ablation front-to-critical density distance. At the same time, electrons that contribute dominant heat flux have an energy of $6.9T_e \approx 12$ keV, and the corresponding range of such electrons becomes 4 μm in a solid PS foil, being a considerable fraction of the target thickness. Consequently, tail electrons in Maxwell distribution may

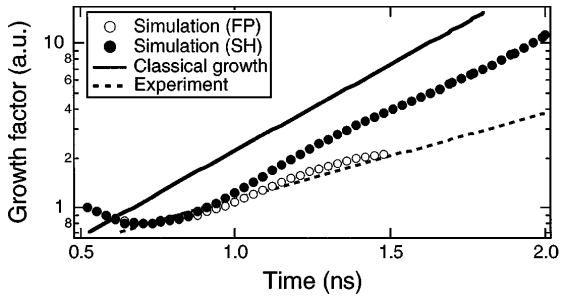

FIG. 5. Growth factor vs time calculated by the 2D simulation code KEICO-2D with the FP treatments for nonlocal heat transport and with the SH treatment for the classical heat transport. Also shown are the classical growth and experimental growth, both of which are identical to those in Fig. 4 except for their arbitral offset.

penetrate into the target, thereby reduce the target density via preheating and thus increase the ablation velocity.

In the following, we will test whether this interpretation is reasonable or not by using a two-dimensional Eulerian simulation code "KEICO-2D" [22]. This code solves either FP equation for the nonlocal electron heat transport or SH equation with the flux limiter of $f = 0.1$ for classical heat transport. The laser energy is dumped at the critical density region in both cases. The top flattening of electron velocity distribution [23] at the laser-absorption region is taken into account in the FP case. The simulation may not correctly treat the nonlocal effect at the early time because the temperature scale length becomes much shorter than the electron mean-free path. Instead, the simulation was run with the SH conduction until the steady state structure of the ablation front is established after the shock breakout at ≈ 0.3 ns, then the FP transport was turned on at 0.5 ns. The density perturbation of 0.1% was introduced at this time [24]. Figure 5 shows the growth factors from the simulation code with two cases: open circles are calculated with the FP equation, and closed circles calculated with the SH equation. The initial small decreases of the perturbation is due to the lateral fluid motion before the RT mode is established. The growth rate was then observed for $t > 0.9$ ns by exponential regression to be 1.4 ns^{-1} for the FP case, and 2.1 ns^{-1} for the SH case. The experimental results are in closer agreement with the simulation results of the FP case than those of the SH case. Indeed, the peak of the target density calculated by KEICO-2D is significantly reduced for the FP case from that for the SH case. The density of the ablation front was calculated to be $1.5-1.7$ g/cm^3 for the FP case, and $2.0-2.4$ g/cm^3 for the SH case, respectively. It appears, therefore, that the observed reduction of the RT growth may be predominantly due to ablative stabilization enhanced by nonlocal heat transport. Further work is necessary to rigorously compare simulations with the experimental results.

In summary, we have shown the first imprint-free measurements of laser-driven Rayleigh-Taylor instability in the linear growth regime. The growth rate is reduced to be 50% of the classical value. Experimental results were compared with the predictions by the two-dimensional computer simulation code. The experimental results are in considerably better agreement with calculations with the nonlocal heat transport rather than those with the classical heat conduction. This implies that the nonlocal electron heat transport plays an important role for the suppression of Rayleigh-Taylor instability at the ablation front.

We acknowledge technical supports by the staffs at ILE Osaka University for the laser operation, target fabrication, and plasma diagnostics.

[1] S. Chandrasekhar, *Hydrodynamic and Hydromagnetic Stability* (Oxford Univ. Press, London, 1968), Chap. 10.
[2] J. Nuckolls *et al.*, Nature (London) **239**, 139 (1972).
[3] T. Shigeyama and K. Nomoto, Astrophys. J. **360**, 242 (1990); W. Arnett *et al.*, Astrophys. J. **341**, L63 (1989).
[4] R. McCrory *et al.*, Phys. Rev. Lett. **46**, 336 (1981); S. Haan, Phys. Rev. A **39**, 5812 (1989).
[5] S. Bodner, Phys. Rev. Lett. **33**, 761 (1974).
[6] H. Takabe *et al.*, Phys. Fluids **28**, 3676 (1985).
[7] B. Remington *et al.*, Phys. Rev. Lett. **67**, 3259 (1991); Phys. Fluids B **4**, 957 (1992).
[8] A. Raven *et al.*, Phys. Rev. Lett. **47**, 1049 (1981); J. Cole *et al.*, Nature (London) **299**, 329 (1982); J. Grun *et al.*, Phys. Rev. Lett. **58**, 2672 (1987); H. Nishimura *et al.*, Phys. Fluids **31**, 2875 (1988); M. Desselberger *et al.*, Phys. Rev. Lett. **65**, 2997 (1990); S. Glendinning *et al.*, Phys. Rev. Lett. **69**, 1201 (1992).
[9] J. Knauer *et al.*, Bull. Am. Phys. Soc. **39**, 1640 (1991).
[10] H. Nakano *et al.*, Appl. Phys. Lett. **63**, 580 (1993).
[11] A. Bell *et al.*, Phys. Rev. Lett. **46**, 243 (1981).
[12] L. Spitzer and R. Härm, Phys. Rev. **89**, 977 (1953).
[13] K. Shigemori *et al.*, *Annual Report of Institute of Laser Engineering* (Osaka University, Osaka, Japan, 1995), p. 135.
[14] N. Miyanaga *et al.*, in *Proceedings of the 15th International Conference on Plasma Phys. Controlled Nucl. Fusion Research* (IAEA, Vienna, 1994); Report No. CN-60/B-P-11 (to be published).
[15] C. Yamanaka *et al.*, Nucl. Fusion **27**, 19 (1987).
[16] Y. Kato *et al.*, Phys. Rev. Lett. **53**, 1057 (1984).
[17] R. Kodama *et al.*, Proc. SPIE **2523**, 165 (1995).
[18] B. Henke *et al.*, At. Data Nucl. Data Tables **54**, No. 2 (1993).
[19] H. Takabe *et al.*, Phys. Fluids **31**, 2884 (1988).
[20] T. Endo *et al.*, Phys. Rev. Lett. **74**, 3608 (1995).
[21] L. Landau and E. Liftshitz, *Fluid Mechanics* (Pergamon, New York, 1987), Sec. 12.
[22] M. Honda *et al.*, in Proceedings of the 24th European Conference on Laser Interaction with Matter, Madrid, 1996 [Report No. PM-7 (to be published)].
[23] A. Langdon *et al.*, Phys. Rev. Lett. **44**, 575 (1980).
[24] E. Emery *et al.*, Phys. Fluids **31**, 1007 (1988).